PERGAMON International Journal of Engineering Science 40 (2002) 693–711

International Journal of Engineering Science

www.elsevier.com/locate/ijengsci

# Application of the "$K$–$\varepsilon$" model to open channel flows in a magnetic field

Sergey Smolentsev [a,*], Mohamed Abdou [a], Neil Morley [a], Alice Ying [a], Tomoaki Kunugi [b]

[a] *Mechanical and Aerospace Engineering Department, Fusion Sciences & Technology Group, University of California, 420 Westwood Plaza, 43-133 Engineering IV, Los Angeles, CA 90095-1597, USA*

[b] *Department of Nuclear Engineering, Kyoto University, Japan*

Received 6 April 2001; received in revised form 20 July 2001; accepted 13 August 2001

**Abstract**

In magnetohydrodynamic (MHD) flows turbulence reduction occurs due to the Joule dissipation. It results in heat transfer degradation. In open channel flows, heat transfer degradation is also caused by the turbulence redistribution near the free surface. Both effects can be significant in fusion applications with low-conductivity fluids such as molten salts. In the present study, the "$K$–$\varepsilon$" model equations for turbulent flows and the free surface boundary condition are adjusted with taking into account MHD effects. Different orientations of the magnetic field, perpendicular and parallel to the main flow, have been considered. The model coefficients have been tuned by a computer optimization using available experimental data for the friction factor. The effect of free surface heat transfer degradation due to the turbulence redistribution has been implemented through the variation of the turbulent Prandtl number. As an example, the model is used for the analysis of a turbulent MHD flow down an inclined chute with the heat flux applied to the free surface. 

*Keywords:* Turbulence; Open channel flow; Heat transfer; Two-equation model; Joule dissipation

## 1. Introduction

In fusion cooling applications, high heat capacity, high thermal conductivity media such as liquid metals are traditionally assumed to be the best working fluids. However due to their high electrical conductivity, liquid metals have strong magnetohydrodynamic (MHD) interaction,

* Corresponding author. Tel.: +1-310-794-5366; fax: +1-310-825-2599.
*E-mail address:* sergey@fusion.ucla.edu (S. Smolentsev).

0020-7225/02/$ - see front matter 
PII: S0020-7225(01)00088-X

which manifests itself through different physical effects. Among these, the most important manifestation is the flow "laminarization" (suppression of turbulence) by a strong magnetic field. Based on the experimental data, the laminarization in channel flows occurs if $Ha/Re > (Ha/Re)_{cr}$, where the Hartmann number, $Ha = B_0 h\sqrt{\sigma/(v\rho)}$, and the Reynolds number, $Re = U_m h/v$, are built using the applied magnetic field, $B_0$, bulk mean velocity $U_m$, characteristic flow dimension $h$, and physical properties of liquid, such as electrical conductivity, $\sigma$, kinematic viscosity, $v$, and density, $\rho$. The critical value of the parameter depends on the magnetic field orientation to the main flow. Because of a strong reactor magnetic field no turbulence models are needed to describe liquid metal MHD flows in fusion devices with the exception of some specific situations.

Along with liquid metals, molten salts are being carefully studied as a practical candidate for fusion applications [1,2]. For example, a 2 cm thick flow of Flibe ($(LiF)_n \cdot (BeF2)$) moving poloidally along the reactor First Wall from the chamber top to the bottom with a velocity of 10 m/s is used in one of the designs of the APEX study [1]. Unlike liquid metals, such flows do not experience significant MHD forces and remain turbulent because electrical conductivity of molten salts is relatively low, about $10^2$ times greater than that of seawater but $10^4$ times less than that of liquid metals. However, under a reactor strong magnetic field, turbulence pulsations in low-conductivity fluids can be partially suppressed with an accompanying reduction in heat transfer. These effects are under consideration in the present study, where the $K$–$\varepsilon$ model of turbulence is adjusted as a numerical tool for analyzing MHD turbulent flows and heat transfer in open channels under the fusion reactor conditions.

In the first studies that modeled MHD wall-bounded turbulence, the Prandtl formula was modified by expressing the dissipation length scale as a function of a magnetic field [3]. Such an approach was realized in [4] by introducing damping factors that stand for the suppression of turbulence by a magnetic field. In more recent studies, two-equation models of turbulence, such as $K$–$\varepsilon$ model [5–8] and RNG models [9] as well as DNS [10,11] and LES [12] were applied to the analysis of some particular MHD turbulent flows in closed channels.

Among two-equation models, which are many in number [13], the standard $K$–$\varepsilon$ model is widely used in engineering applications. However, this model is not directly applied to MHD flows because it does not account for the stabilizing effect of the magnetic field. There are several studies that extend this model to MHD flows in closed channels in a transverse magnetic field (see [5–8]). In one of the first studies using a two-equation model [5], the sink term standing for the Joule dissipation and the destruction term were added to the equations for "$K$" and "$\varepsilon$" in the form of

$$C_3 \frac{\sigma}{\rho} B_0^2 K, \quad C_4 \frac{\sigma}{\rho} B_0^2 \varepsilon, \tag{1}$$

respectively, with the closure constants $C_3 = 0.5$ and $C_4 = 1.0$. Other studies adopting the same approach [7,8] give the closure constants slightly different from those in [5]. In more recent publications, special attention has been paid to introduce anisotropy in the distribution of the turbulent kinetic energy through the variations in $C_3$ and $C_4$ [14,15]. In spite of a recent progress in MHD turbulence modeling none of the modifications in their present form can be considered as universal as the conventional $K$–$\varepsilon$ model for non-MHD flows. Additionally, to our knowledge, no applications of the $K$–$\varepsilon$ model have been known for open channel MHD flows.

Along with the development of universal closures for modeling MHD turbulence, well-tuned engineering models suited for particular applications are needed. In the present study, we focus on

the adjustment of the $K$–$\varepsilon$ model for particular turbulent flows with the magnetic field perpendicular or parallel to the main flow direction. Also, we develop a procedure to modify the free surface boundary conditions [16] that were originally proposed for non-MHD flows.

## 2. Turbulence model

Assuming low magnetic Reynolds number and applying Reynolds averaging to the Navier–Stokes–Maxwell equations with the conventional closure approximations, one can obtain equations for the turbulent kinetic energy per unit mass, $K$, and the dissipation rate per unit mass, $\varepsilon$. The transport equation for $K$ is derived here by the conventional method. After decomposing the velocity into the mean and fluctuating parts, each of the equations for the fluctuating parts is multiplied by the corresponding pulsation velocity component. Then, the equations obtained are added together and averaged. Finally, unknown turbulent correlations are replaced by algebraic expressions with closure coefficients. Doing all these steps results in the equation for $K$ as follows:

$$\frac{\partial K}{\partial t}+\langle v_j\rangle\frac{\partial K}{\partial x_j}=\underbrace{\nu_{\mathrm{t}}\left(\frac{\partial\langle v_i\rangle}{\partial x_j}\right)^2}_{\text{Production}}+\underbrace{\frac{\partial}{\partial x_j}\left[\left(\nu+\frac{\nu_{\mathrm{t}}}{\sigma_K}\right)\frac{\partial K}{\partial x_j}\right]}_{\text{Diffusion}}-\underbrace{\varepsilon-\varepsilon_{\mathrm{em}}^K}_{\text{Dissipation}}. \tag{2}$$

The first three terms on the RHS of Eq. (2) are standard, while the fourth one, $\varepsilon_{\mathrm{em}}^K$, is electromagnetic. The expression for $\varepsilon_{\mathrm{em}}^K$ is obtained by the above procedure and comes from the $\vec{j}'\times\vec{B}_0=\sigma(-\nabla\varphi'+\vec{v}'\times\vec{B}_0)\times\vec{B}_0$ term on the RHS of the momentum equation for the fluctuating velocity as follows:

$$\varepsilon_{\mathrm{em}}^K=D_{\mathrm{I}}+D_{\mathrm{II}}=\underbrace{\frac{\sigma}{\rho}\left(2B_0^2K-B_{0i}B_{0k}\langle v_i'v_k'\rangle\right)}_{D_{\mathrm{I}}}+\underbrace{\frac{\sigma}{\rho}\varepsilon_{ijk}B_k\left\langle\frac{\partial\varphi'}{\partial x_j}v_i'\right\rangle}_{D_{\mathrm{II}}}, \tag{3}$$

where $\varepsilon_{ijk}$ is the Levi–Civita symbol defined by

$$\varepsilon_{ijk}=\begin{cases}+1 & \text{if } (i,j,k) \text{ are cyclic,}\\ -1 & \text{if } (i,j,k) \text{ are anticyclic,}\\ 0 & \text{otherwise.}\end{cases}$$

The relationship between $K$, $\varepsilon$, and the eddy viscosity, $\nu_{\mathrm{t}}$, is given by the Kolmogorov–Prandtl expression: $\nu_{\mathrm{t}}=C_\nu K^2/\varepsilon$ with $C_\nu$ as a model coefficient. The exact equation for $\varepsilon$ can also be derived. However following the general practice, the standard model equation for $\varepsilon$ is best viewed as being entirely empirical [17]: it is

$$\frac{\partial\varepsilon}{\partial t}+\langle v_j\rangle\frac{\partial\varepsilon}{\partial x_j}=C_1\frac{\varepsilon}{K}\nu_{\mathrm{t}}\left(\frac{\partial\langle v_i\rangle}{\partial x_j}\right)^2+\frac{\partial}{\partial x_j}\left[\left(\nu+\frac{\nu_{\mathrm{t}}}{\sigma_\varepsilon}\right)\frac{\partial\varepsilon}{\partial x_j}\right]-C_2\frac{\varepsilon}{K}\varepsilon-\varepsilon_{\mathrm{em}}^{\varepsilon}. \tag{4}$$

Similar to Eq. (2) the last one also includes the electromagnetic term, $\varepsilon^{\varepsilon}_{\mathrm{em}}$, which is not necessarily the same as that in (2). In Eqs. (2) and (4), $C_1$, $C_2$, $\sigma_K$, and $\sigma_\varepsilon$ are the conventional closure coefficients. The production term in both equations is given in a simplified form, which is appropriate for channel flows. The essence of the turbulence model is how to model the electromagnetic terms. The analysis of the sink term, $\varepsilon^{K}_{\mathrm{em}}$, and the closure relation are given below. In modeling the destruction term, $\varepsilon^{\varepsilon}_{\mathrm{em}}$, we used the commonly accepted approach (see [5,7,8]), whereby the closure form for this term is adopted from that for $\varepsilon^{K}_{\mathrm{em}}$.

Expression (3) includes terms with velocity pulsations ($D_{\mathrm{I}}$) and velocity – electric field fluctuations ($D_{\mathrm{II}}$), which come from two components in Ohm's law: $\sigma\vec{V}'\times\vec{B}_0$ and $-\sigma\nabla\varphi'$, respectively. The term $D_{\mathrm{I}}$ is always positive, while $D_{\mathrm{II}}$ is negative. Although the ratio between $D_{\mathrm{I}}$ and $D_{\mathrm{II}}$ can vary in a wide range depending on the flow parameters, their sum, $\varepsilon^{K}_{\mathrm{em}}$, which stands for the Joule dissipation, is always positive. In what follows, we will restrict ourselves to examining the effect of a one-component magnetic field. Table 1 gives $D_{\mathrm{I}}$ and $D_{\mathrm{II}}$ for these particular cases. In the table and below, $x$, $y$ and $z$ are the streamwise, wall-normal and spanwise coordinate, respectively.

To model $\varepsilon^{K}_{\mathrm{em}}$ one can draw on the following generally observed tendency. The distribution of $D_{\mathrm{II}}$ is similar in shape to that of $D_{\mathrm{I}}$ and both are similar in shape to the distribution of $K$. An example based on DNS data for a fully developed turbulent flow between two parallel walls with a wall-normal magnetic field [10] is shown in Fig. 1. The DNS data for channel flows in a streamwise magnetic field [10] and those for free surface flows in a spanwise magnetic field [18] demonstrate the same feature. This gives a ground to model $\varepsilon^{K}_{\mathrm{em}}$ in the form given by (1) with $C_3$ depending on the field orientation as well as local or bulk flow parameters.

In channel flows with a weak magnetic field ($Ha/Re \ll (Ha/Re)_{\mathrm{cr}}$) perpendicular to the main flow, the turbulence structure is close to that in ordinary flows where streamwise vortices dominate. For such flows, the Joule dissipation is mostly contributed by $D_{\mathrm{I}}$. Taking into accounts that $\langle v'v'\rangle, \langle w'w'\rangle < \langle u'u'\rangle$ and $2K = \langle u'u'\rangle + \langle v'v'\rangle + \langle w'w'\rangle$ one can arrive at the following approximation: $\varepsilon^{K}_{\mathrm{em}} \approx C_3\sigma/\rho B_0^2 K$ with $C_3$ of about 2. In another particular case of a strong magnetic field perpendicular to the main flow, transition to a 2D state occurs, in which turbulent eddies are elongated in the field direction, so that $D_{\mathrm{I}}$ and $D_{\mathrm{II}}$ become nearly equal in magnitude but opposite in sign and $\varepsilon^{K}_{\mathrm{em}} \to 0$. Therefore in cases with a magnetic field perpendicular to the main flow direction, $C_3$ drops from about 2 to a smaller value as the magnetic field grows. In the present study, we adopt an exponential approximation for $C_3$ similar to that in [15] for pipe MHD flows, where

Table 1
Specification of electromagnetic term $\varepsilon^{K}_{\mathrm{em}}$ for a one-component magnetic field

| $\vec{B}_0$ | $D_{\mathrm{I}}$ | $D_{\mathrm{II}}$ |
|---|---|---|
| $(B_{0x},0,0)$ (streamwise) | $\frac{\sigma}{\rho}B_{0x}^2(\langle v'v'\rangle + \langle w'w'\rangle)$ | $\frac{\sigma}{\rho}B_{0x}\left(\left\langle\frac{\partial\varphi'}{\partial z}v'\right\rangle - \left\langle\frac{\partial\varphi'}{\partial y}w'\right\rangle\right)$ |
| $(0,B_{0y},0)$ (wall-normal) | $\frac{\sigma}{\rho}B_{0y}^2(\langle u'u'\rangle + \langle w'w'\rangle)$ | $\frac{\sigma}{\rho}B_{0y}\left(\left\langle\frac{\partial\varphi'}{\partial x}w'\right\rangle - \left\langle\frac{\partial\varphi'}{\partial z}u'\right\rangle\right)$ |
| $(0,0,B_{0z})$ (spanwise) | $\frac{\sigma}{\rho}B_{0z}^2(\langle u'u'\rangle + \langle v'v'\rangle)$ | $\frac{\sigma}{\rho}B_{0z}\left(\left\langle\frac{\partial\varphi'}{\partial y}u'\right\rangle - \left\langle\frac{\partial\varphi'}{\partial x}v'\right\rangle\right)$ |

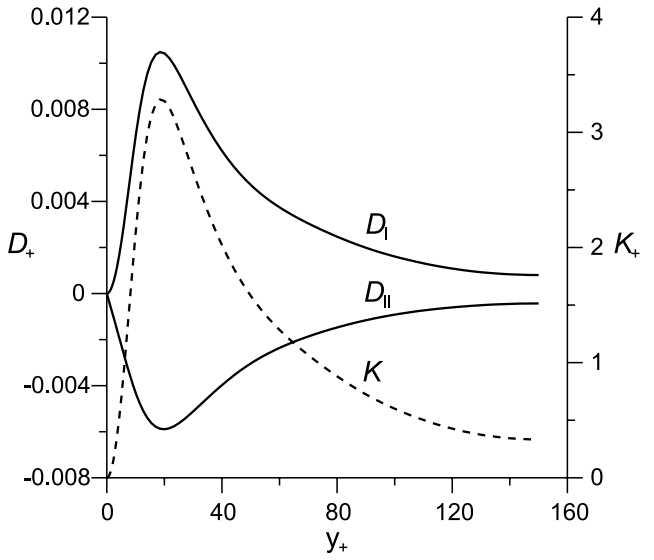


Fig. 1. Distributions of the $D_{\mathrm{I}}$ and $D_{\mathrm{II}}$ terms entering the expression (3) for the Joule dissipation and the turbulence kinetic energy distribution in fully developed MHD flow between parallel walls with a wall-normal magnetic field [10]: $Ha = 6;\ Re_\tau = 150$.

$C_3 \sim \exp\{-N\}$ and $N = Ha^2/Re$ is the interaction parameter. The details of implementation of the present model and the numerical values of closure parameters are different from those given in [15].

In a streamwise magnetic field, the turbulence structure is less severely affected by the field and the degree to what the turbulence is suppressed by the field is much less. That is because unlike the cases with a wall-normal or spanwise magnetic field, the streamwise field does not directly interact with the streamwise velocity pulsations. The indirect interaction occurs through changing the pressure distribution. Also, the streamwise velocity does not enter the expressions for $D_{\mathrm{I}}$, $D_{\mathrm{II}}$ implicitly. In terms of the turbulence closure, this means smaller values of $C_3$ and its reduced sensitivity to the magnetic field variation. The specification of additional terms along with the closure constants evaluated through the experimental data for the different field orientations is shown in Table 2.

The evaluation of the closure constants have been performed using well-documented sets of the experimental data for the friction factor in MHD flows in slotted channels (wall-normal and spanwise magnetic field) and in pipes (streamwise magnetic field). In the calculations, the low-Reynolds number corrections of the $K$–$\varepsilon$ model were used to provide accurate results when integrating through the viscous sublayer. The details of the low-Reynolds number model are given in the following section. When adjusting the model coefficients, the following set of mean equations for fully developed flows was used:

$$0 = -\frac{1}{\rho}\frac{\mathrm{d}P}{\mathrm{d}x} + \frac{\mathrm{d}}{\mathrm{d}y}\left[\nu(1+\varepsilon_{\mathrm{t}})\frac{\mathrm{d}U}{\mathrm{d}y}\right] + \frac{f_{\mathrm{em}}}{\rho},$$

$$\int_0^h U(y)\,\mathrm{d}y = Q.$$

Table 2
Specification of the electromagnetic terms in equations for $K$ and $\varepsilon$ after modeling

| Magnetic field direction | $\varepsilon_{\mathrm{em}}^{K}$ | $\varepsilon_{\mathrm{em}}^{\varepsilon}$ | $C_3$ | $C_4$ | Experimental data used |
|---|---|---|---|---|---|
| Streamwise | $C_3\frac{\sigma}{\rho}B_0^2K$ | $C_4\frac{\sigma}{\rho}B_0^2\varepsilon$ | 0.02 | 0.015 | [19,20] |
| Wall-normal | $C_3\frac{\sigma}{\rho}B_0^2K$ | $C_4\frac{\sigma}{\rho}B_0^2\varepsilon$ | $1.9\exp\{-1.0N\}$ | $1.9\exp\{-2.0N\}$ | [21] |
| Spanwise | $C_3\frac{\sigma}{\rho}B_0^2K$ | $C_4\frac{\sigma}{\rho}B_0^2\varepsilon$ | $1.9\exp\{-1.0N\}$ | $1.9\exp\{-2.0N\}$ | [22] |

Here, $\varepsilon_{\mathrm{t}}$ is the dimensionless eddy viscosity, $\varepsilon_{\mathrm{t}} = \nu_{\mathrm{t}}/\nu$. The second of the equations provides a fixed volumetric flux, $Q$, through the channel. The electromagnetic term, $f_{\mathrm{em}}$, which stands for the mean Lorenz force, depends on the magnetic field orientation:

$$f_{\mathrm{em}} = \begin{cases} 0 & \text{spanwise or streamwise magnetic field,} \\ -\sigma B_{0y}(U - U_{\mathrm{m}}) & \text{wall-normal magnetic field.} \end{cases}$$

In the case of a wall-normal magnetic field, the non-zero electromagnetic force results in the so-called ''Hartmann effect''. The flow near the walls within the Hartmann layers is accelerated, while it is slowed down in the balk. This results in flattening the velocity profile. The model coefficients in the case of a streamwise magnetic field were adjusted using experimental data for pipe flows (experimental data for rectangular channel flows in a streamwise magnetic field are not available). The same mean flow equations but written in cylindrical coordinates were applied. The mean flow equations for developing open channel flows as well as the details of the numerical method used in the calculations are given in Section 5.

The model reproduces the experimental data for a streamwise magnetic field with the accuracy of $\pm 10\%$. The calculated friction factor results for two other cases are plotted in Figs. 2 and 3, respectively, against the experimental data. Here and in what follows, the dimensionless parameters are built through the dimension $h$ (the closed channel width or the open channel flow depth) and the mean bulk velocity, $U_{\mathrm{m}}$. Usually using bulk parameters is not a conventional approach in turbulence modeling. Nevertheless a good agreement has been achieved because in flows with a relatively simple geometry like those in channels, the large energy containing eddies have a length scale close to the characteristic dimension of a channel. As it can be seen from Table 2, the same model specification can be used for two perpendicular orientations, while the specification for the streamwise field is different that emphasizes differences between the mechanisms of turbulence suppression depending on the magnetic field orientation. Although the same closure coefficients are used for spanwise and wall-normal fields, it does not automatically mean the same degree of turbulence suppression. The latter has a stronger effect, which is explained by flattening the velocity profile due to the Hartmann effect. Illustrations of the magnetic field effect on turbulent quantities for the wall-normal magnetic field (with the Hartmann effect) and the spanwise magnetic field (without the Hartmann effect) in open channel flows are given in subsequent sections.

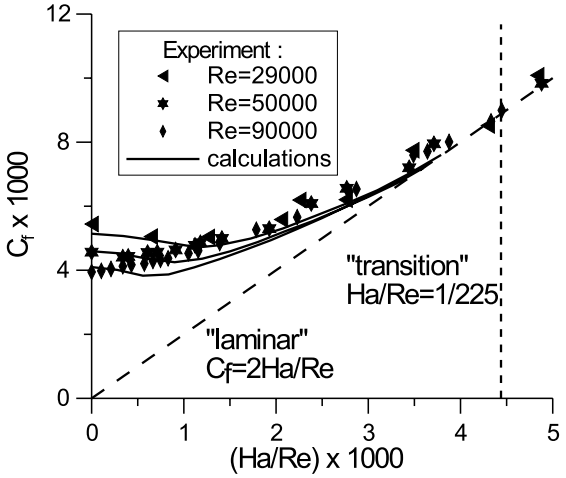


Fig. 2. Experimental [21] and calculated friction factor results for a wall-normal magnetic field.

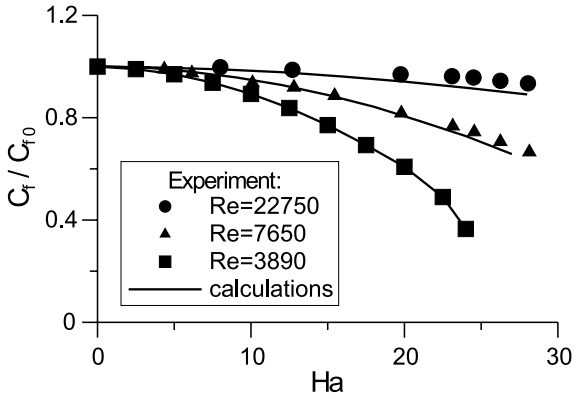


Fig. 3. Experimental [22] and calculated friction factor results for a spanwise magnetic field.

## 3. Low-Reynolds number model

The present turbulence model has the same weakness as the standard one. Namely, it is restricted to high-Reynolds number applications and it fails to predict adequately the mean flow profile near the solid wall, where viscous effects are predominant over turbulent ones. Hence, to provide accurate predictions of the flow down to the wall, the model needs to be modified. In the present approach, we used the low-Reynolds number method. To our knowledge, there are no experimental results for the distributions of turbulent quantities near the wall in MHD flows, since such measurements are extremely difficult. However, there exists some data of DNS and LES calculations, though these are few in number (see [10–12,18]). These data indicate to a certain extent that the structure of the near wall turbulence does not undergo significant changes even though the influence of the magnetic field on the mean flow is pronounced. It gives grounds to use

one of the low-Reynolds number modifications, which are widely used in usual practice of turbulence modeling for non-MHD flows.

No consensus has been achieved on the optimum form of the low-Reynolds number equations as evidenced by a large number of different versions of the model [23]. In this study, preference has been given to the low-Reynolds number turbulence model in the form proposed by Chien [24]. This form is consistent with the turbulence asymptotic analysis within the viscous sublayer and gives better predictions of the peak turbulent kinetic energy at the wall for channel and boundary layer flows than the other models including the classical one of Jones and Launder [25].

The general form of the low-Reynolds number model for a fully developed MHD flow can be written compactly as follows:

$$0 = \frac{\mathrm{d}}{\mathrm{d}y_+}\left[\left(1+\frac{\varepsilon_\mathrm{t}}{\sigma_k}\right)\frac{\mathrm{d}K_+}{\mathrm{d}y_+}\right] + \varepsilon_\mathrm{t}\left(\frac{\mathrm{d}U_+}{\mathrm{d}y_+}\right)^2 - \tilde{\varepsilon}_+ - \varepsilon_{+0} - C_3\frac{Ha^2}{Re_\tau^2}K_+, \tag{5}$$

$$0 = \frac{\mathrm{d}}{\mathrm{d}y_+}\left[\left(1+\frac{\varepsilon_\mathrm{t}}{\sigma_\varepsilon}\right)\frac{\mathrm{d}\tilde{\varepsilon}_+}{\mathrm{d}y_+}\right] + C_1 f_1 \varepsilon_\mathrm{t}\frac{\tilde{\varepsilon}_+}{K_+}\left(\frac{\mathrm{d}U_+}{\mathrm{d}y_+}\right)^2 - C_2 f_2\frac{\tilde{\varepsilon}_+^2}{K_+} + E - C_4\frac{Ha^2}{Re_\tau^2}\tilde{\varepsilon}_+. \tag{6}$$

The equations are normalized using the wall units. The dissipation rate, $\varepsilon_+$, is related to the quantity $\tilde{\varepsilon}_+$ by

$$\varepsilon_+ = \varepsilon_{+0} + \tilde{\varepsilon}_+. \tag{7}$$

The quantity $\varepsilon_{+0}$ is the value of $\varepsilon_+$ at the wall, and $f_1$, $f_2$ and $E$ are the empirical damping functions. One more damping function, $f_v$, is introduced into the expression for the eddy viscosity, so that

$$\varepsilon_\mathrm{t} = C_v f_v\frac{K_+^2}{\tilde{\varepsilon}_+}. \tag{8}$$

In the Chien model

$$\begin{aligned}
&f_v = 1-\exp\{-C_{\mathrm{Ch}3}y_+\},\\
&f_1 = 1,\\
&f_2 = 1-0.22\exp\{-(Re_\mathrm{T}/6)^2\}, \quad Re_\mathrm{T} = \frac{K_+^2}{\tilde{\varepsilon}_+},\\
&\varepsilon_{+0} = 2K_+/y_+^2,\\
&E = -2\frac{\tilde{\varepsilon}_+}{y_+^2}\exp\{-C_{\mathrm{Ch}4}y_+\},\\
&C_1 = 1.35, \quad C_2 = 1.80, \quad C_v = 0.09, \quad \sigma_k = 1.0, \quad \sigma_\varepsilon = 1.3, \quad C_{\mathrm{Ch}3} = 0.0115, \quad C_{\mathrm{Ch}4} = 0.5.
\end{aligned} \tag{9}$$

The boundary condition at the wall when solving (5) and (6) in the near-wall region is $K_+ = 0$ and $\tilde{\varepsilon}_+ = 0$. The free surface boundary condition is discussed in the following section.

## 4. Free surface boundary condition

In the first studies of turbulent flows in open channels, the "rigid-lid" surface was assumed to act like a plane of symmetry (see, for example, [26]). The symmetry condition requires that both $K$ and $\varepsilon$ have zero $y$-gradient at the surface:

$$\left(\frac{\partial K}{\partial y}\right)_s = 0; \quad \left(\frac{\partial \varepsilon}{\partial y}\right)_s = 0. \tag{10}$$

However using such conditions results in overestimated values for $K$ and $\nu_t$ near the surface. More accurate free surface boundary condition based on the experimental data were proposed by Hossain and Rodi [16]:

$$\left(\frac{\partial K}{\partial y}\right)_s = 0; \quad \varepsilon_s = \frac{C_\nu^{3/4} K_s^{3/2}}{0.07 h\kappa}. \tag{11}$$

The second of (11) expresses the fact that the dissipation length scale at the free surface is about 7% of the flow thickness:

$$l_s = 0.07h \tag{12}$$

where $l$ is defined as $l = C_\nu^{3/4} K^{3/2} \varepsilon^{-1} \kappa^{-1}$ and $\kappa$ is the von Karman constant. This boundary condition gives a well-known "parabolic" distribution of $\nu_t$ with the maximum at about halfway between the wall and the free surface. However, a magnetic field rapidly changes the dissipation length scale, so that (12) is applicable only in a very low field. One can expect shortening $l_s$ as the field grows. To incorporate MHD effects we used the following modification of (11). First, two new quantities, $l_{s1}$ and $l_{s0}$, were calculated as the dissipation length scales at the free surface with and without a magnetic field, respectively, using the symmetry boundary condition (10). The decrease of the parameter $l_{s1}/l_{s0}$ as the Hartmann number grows is shown in Fig. 4. Then, modified $l_s$ was introduced in (11) in the form of $l_s = 0.07h \times l_{s1}/l_{s0}$ that results in

$$\left(\frac{\partial K}{\partial y}\right)_s = 0; \quad \varepsilon_s = \frac{C_\nu^{3/4} K_s^{3/2}}{0.07 h\kappa} \frac{l_{s0}}{l_{s1}}. \tag{13}$$

Some examples of applying different boundary conditions are shown in Fig. 5. Using (13) provides reasonable physical behavior of the eddy viscosity as a magnetic field grows while applying the symmetry boundary condition or boundary condition (12) leads to the overestimation of $\nu_t$. In a strong magnetic field, flow laminarization occurs. First, the flow becomes laminarized near the free surface. For such flows better boundary condition is given by (10). Based on the calculations, the symmetry boundary condition could be recommended if the parameter $Ha/Re$ exceeds about $1.5\times10^{-2}$, $8.0 \times 10^{-4}$ and $2.0 \times 10^{-3}$ for a streamwise, wall-normal and spanwise magnetic field, respectively. For comparison, $(Ha/Re)_{cr}$ at which flow laminarization occurs in closed channel flows in the whole area for these cases is $2.5 \times 10^{-2}$ [27], $4.5 \times 10^{-3}$ [21] and $8.0 \times 10^{-3}$ [22], respectively.

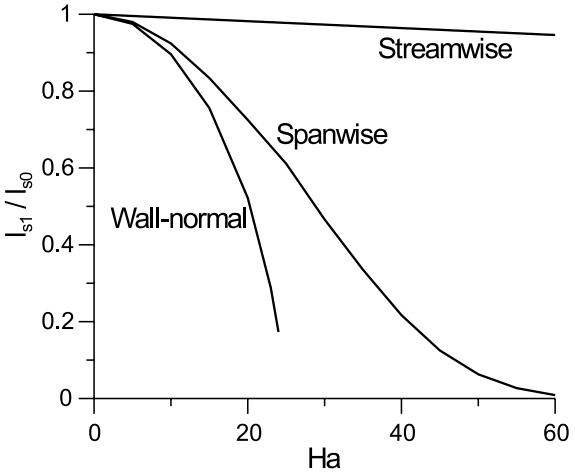


Fig. 4. Decrease of the dissipation length scale at the free surface under the influence of a magnetic field: $Re = 30000$.

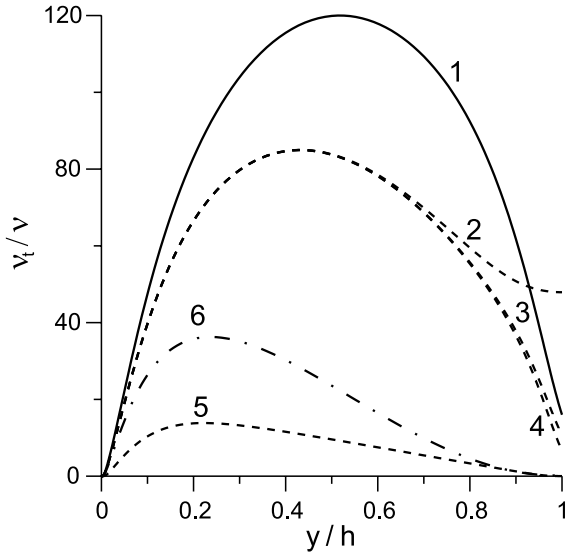


Fig. 5. Distributions of the eddy viscosity in open channel MHD flow calculated with different free surface boundary conditions: 1 – $Ha = 0$, Hossain and Rodi BC (11); 2 – $Ha = 25$, spanwise magnetic field, symmetry BC (10); 3 – $Ha = 25$, spanwise magnetic field, Hossain and Rodi BC (11); 4 – $Ha = 25$, spanwise magnetic field, modified Hossain and Rodi BC (13); 5 – $Ha = 60$, spanwise magnetic field, symmetry BC (10); 6 – $Ha = 25$, wall-normal magnetic field, symmetry BC (10).

## 5. Free surface flow in an inclined chute

As an application, a turbulent flow down a chute in a spanwise or wall-normal magnetic field has been calculated. The chute flow is defined as a free surface flow down an inclined flat surface (with $\alpha$ as a chute inclination angle with respect to the horizon) bounded by two side-walls. In

what follows, we assume the chute aspect ratio (the chute width over the characteristic flow height) to be large. This allows two-dimensional formulation since effects at the side-walls do not affect significantly the flow bulk. In spite of its simplicity, such a problem can serve as a model for a film flow of a low-conductivity fluid over the divertor plate in a strong magnetic field in a fusion reactor. At the same time it could be a good basis for verifying the model itself by comparing the experimental and calculated flow thickness. Such measurements are relatively simple and can be done with a good accuracy, for example using ultrasound transducers.

The mathematical formulation includes Reynolds-averaged flow equations for a non-steady-state developing flow written in the boundary layer approximation along with the present turbulence model and the modified free surface boundary condition. Unlike the expressions for $C_3$ and $C_4$ in Table 2, the following modifications were used:

$$C_3 = 1.9\exp\{-2.0N\}, \quad C_4 = 1.9\exp\{-4.0N\}.$$

Doubling the power is introduced here because from the geometrical viewpoint, the open channel flow with the depth $h$ is similar to that in a closed channel with the width $2h$. The mean equations being solved are written in the Cartesian coordinates with the $x$-axis (streamwise direction) in the main flow direction, the $y$-axis (wall-normal direction) perpendicular to the wall, and the coordinate origin located on the wall in the inlet cross-section, as follows:

$$\frac{\partial U}{\partial t} + U\frac{\partial U}{\partial x} + V\frac{\partial U}{\partial y} = -g\cos(\alpha)\frac{\partial h}{\partial x} + g\sin(\alpha) + \frac{\partial}{\partial y}\left[\nu(1+\varepsilon_t)\frac{\partial U}{\partial y}\right] + \frac{f_{em}}{\rho},$$

$$\frac{\partial U}{\partial x} + \frac{\partial U}{\partial y} = 0,$$

$$\frac{\partial h}{\partial t} + U_s\frac{\partial h}{\partial x} = V_s.$$

Two first equations are used to calculate the velocity components. The third of the equations, the kinematic free surface condition, is used to calculate the local flow thickness, $h(t,x)$. The boundary conditions are the no-slip conditions at the wall and no-tangential stress at the free surface.

The equations were approximated with the finite-difference formulas using a stretched grid, which concentrates grid points near the wall and the surface. To provide proper resolution in the wall vicinity, the number of grids across the flow was 50–200 depending on the turbulence Reynolds number, with the first grid point located between $y_+ = 0.1$ and $y_+ = 0.5$. The solution was sought as a steady-state of a time-dependent problem using a Blottner-type finite-difference method [28] with a surface height method as a technique for tracking the free surface.

To validate the model and the code in a non-MHD case, several comparisons with the data available for open channel flows have been made. First, the fully developed velocity profile was calculated and plotted (Fig. 6) against the viscous sublayer velocity profile, $U_+ = y_+$, the log-law, $U_+ = \ln(y_+)/\kappa + A$, and Cole's extension of the log-low in the outer region, $U_+ = \ln(y_+)/\kappa + A + W(y/h)$ [29]. Second, the mixing length (Fig. 7) was plotted against the experimental data [30]. Both tests demonstrate a reasonable agreement. Unfortunately, any experimental data suitable for the comparison on open channel flows in a magnetic field have not been available.

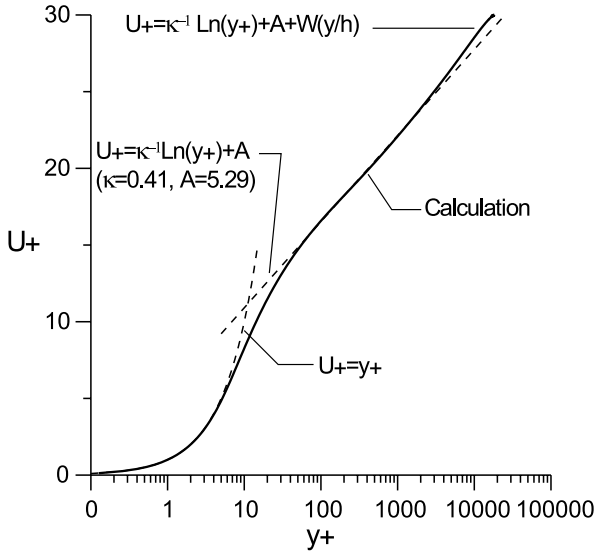


Fig. 6. Test 1. Calculated against theoretical velocity profile [29] in open channel flow without a magnetic field: $Re = 500\,000$.

In accordance with [29], the turbulent structure of open channel flows can be subdivided into three subregions: the wall region ($y/h < 0.15$–$0.2$), the intermediate region ($0.15$–$0.2 < y/h < 0.6$), and the free surface region ($0.6 < y/h < 1.0$). The first two subregions are almost not influenced by the free surface and are the same as the viscous sublayer and the log-layer in the near-wall turbulent flows, respectively. In the free surface region, the turbulent energy is supplied from the

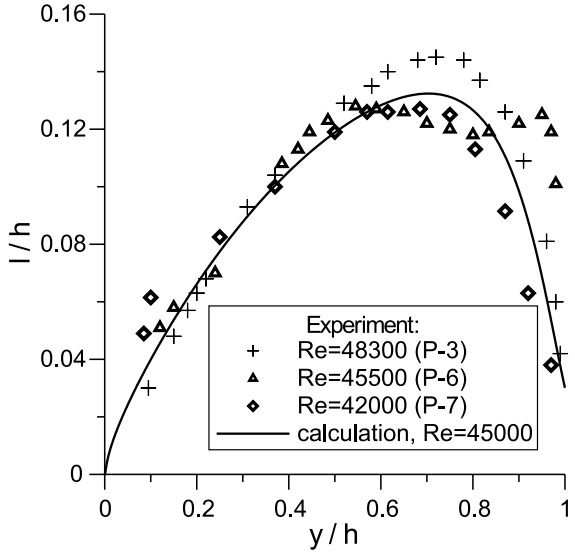


Fig. 7. Test 2. Calculated against experimental [30] dissipation length scale in open channel flow without a magnetic field.

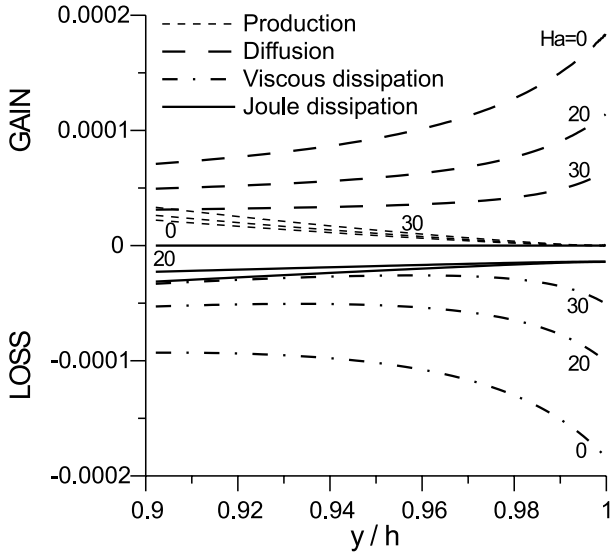


Fig. 8. Budget of the turbulence kinetic energy in the free surface region of a chute MHD flow in a spanwise magnetic field: $Re = 30\,000$.

wall region by turbulent diffusion and dissipated due to the viscosity effect. In this region, the dissipation rate prevails over the turbulence production. There is a local growth of $\varepsilon$ directly near the free surface. In the presence of a magnetic field, as it is evidenced by the present calculations (Fig. 8), the same trend toward a higher viscous dissipation near the surface is observed. At the same time, the contribution of the viscous dissipation is reduced, while that of the Joule dissipation grows as the magnetic field grows. The turbulence production in this region is small and slightly affected by the magnetic field.

Although a magnetic field leads to turbulence suppression in all cases, the degree and the nature of suppression can vary. These variations can be seen from the kinetic energy distributions (Fig. 9) and velocity profiles (Fig. 10). Both cases demonstrate turbulence reduction in the whole region, while the case of a wall-normal magnetic field is characterized by a stronger reduction of turbulence especially in the free surface region because of flattening the velocity profile due to the Hartmann effect. As a magnetic field grows, flow laminarization occurs in the free surface region first, while turbulence still persists in the shear layer near the wall. Ultimately, the flow over the whole area becomes laminar. In the case of a spanwise field, laminarization is not so strong, since the Hartmann effect is not present. The velocity profiles in the free surface region become less flattened approaching to parabolic ones in a laminar non-MHD flow.

## 6. Heat transfer

There are two mechanisms related to turbulence, which affect heat transfer in a free surface MHD flow. First, heat transfer degradation takes place due to suppression of turbulent pulsations through the Joule dissipation. This mechanism affects the whole flow region. The second mechanism

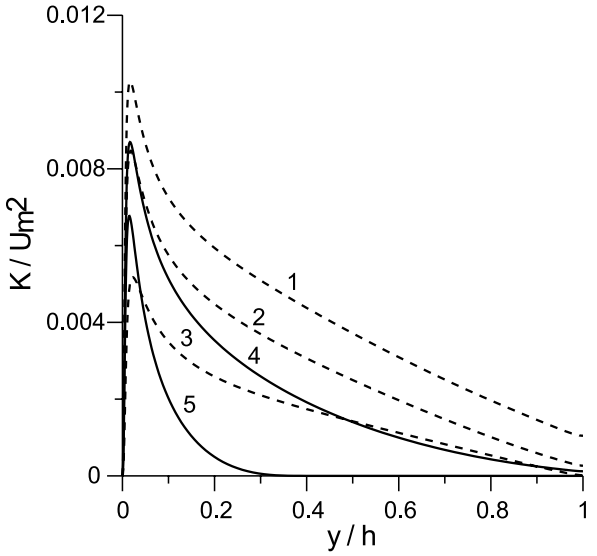


Fig. 9. Distributions of the turbulence kinetic energy in a chute MHD flow: $Re = 30000$. 1 – $Ha = 0$; 2 – $Ha = 30$, spanwise magnetic field; 3 – $Ha = 50$, spanwise magnetic field; 4 – $Ha = 20$, wall-normal magnetic field; 5 – $Ha = 40$, wall-normal magnetic field.

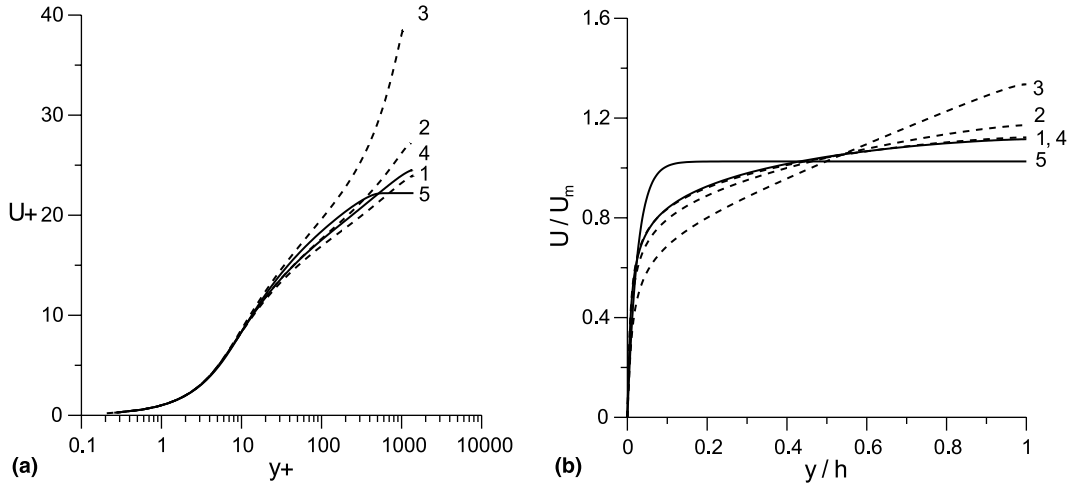


Fig. 10. Velocity profiles in a chute MHD flow plotted with universal (a) and outer (b) scaling: $Re = 30000$. See notation in Fig. 9.

manifests itself only in free surface flows and is caused by the turbulence redistribution in the free surface region. There has been much experimental and numerical evidence of the turbulent structure change in this region. Unless a surface renewal occurs or surface turbulence is generated by the wind shear, the velocity pulsations normal to the surface are suppressed, while the other two components are enhanced due to continuity [31,32]. Hence, in the presence of a free surface, 3D

bulk turbulence degenerates into a specific surface turbulence, in which turbulent vortices are attached to the surface. Such vortices are two-dimensional at the surface (the rotation occurs in the free surface plane) and do not enhance heat transfer. It leads one to speak about near-surface flow laminarization in the sense of heat transfer degradation. At the same time, turbulence eddies in the flow bulk almost do not undergo any structural changes. In terms of heat transfer, it means that the thermal resistance is not uniform across the flow and grows in the free surface region reaching its maximum at the surface.

In turbulence modeling of heat transport, the commonly accepted model for the mean turbulent flux is given by the extension of the Fourier law for the heat conduction:

$$\langle t'v' \rangle = -\frac{\nu_t}{Pr_t}\frac{\partial T}{\partial y}. \tag{14}$$

Inclusion of relation (14) into the Reynolds-averaged energy equation incorporates both effects of turbulence on heat transfer: the first one through $\nu_t$ and the second one through $Pr_t$. The turbulent Prandtl number, $Pr_t$, stands for the ratio between the eddy diffusivity for momentum and eddy diffusivity for heat. To describe properly heat transfer degradation in the free surface region, $Pr_t$ should be evaluated from experimental data. In the present study, $Pr_t$ (Fig. 11) was calculated by using the eddy diffusivity for momentum obtained with the $K$–$\varepsilon$ model, while lacking suitable data for free surface MHD flows, the eddy diffusivity for heat was taken from the experiments for open channel water flows [31]. The best fit was found as

$$Pt_t = 0.7 \times (1 + \exp\{37 \times (y/h - 0.89)\}). \tag{15}$$

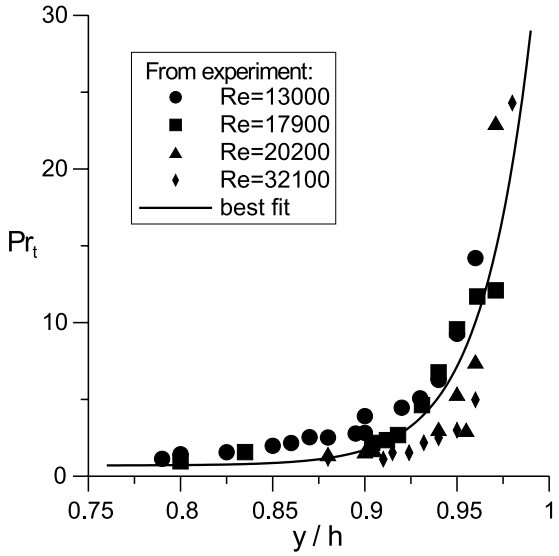


Fig. 11. Distribution of the turbulent Prandtl number in the free surface region of open channel flow based on the experimental data for the eddy diffusivity for heat [31] and present calculations of the eddy diffusivity for momentum.

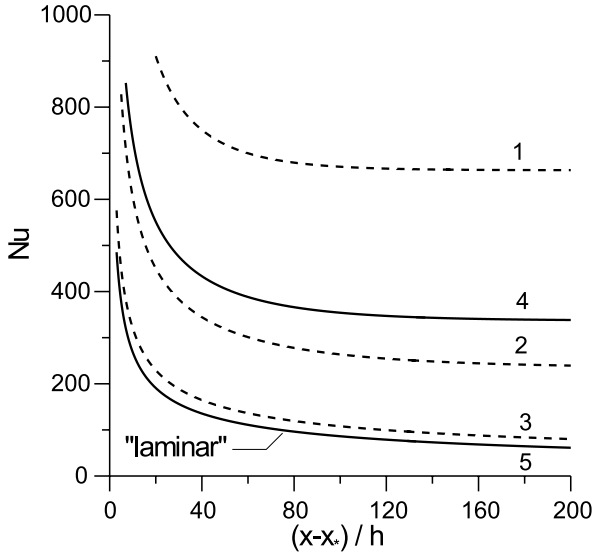


Fig. 12. Nusselt number in a chute MHD flow with the heat flux applied to the free surface: $Re = 30000; Pr = 30$. See notation in Fig. 9.

Using (15), temperature calculations were carried for the same chute flow defined in Section 5 with the uniform heat flux applied to the free surface and no heat flux at the wall over the hydrodynamically fully developed flow region ($x > x_*$). The energy equation being used in the calculations is the following:

$$\rho C_{\mathrm{p}}\left(\frac{\partial T}{\partial t} + U\frac{\partial T}{\partial x} + V\frac{\partial T}{\partial y}\right) = \frac{\partial}{\partial y}\left[k\left(1 + \varepsilon_{\mathrm{t}}\frac{Pr}{Pr_{\mathrm{t}}}\right)\frac{\partial T}{\partial y}\right].$$

The same flow parameters as those given in Section 5 were used (see notation in Fig. 9). The velocity profiles and the distributions of the turbulent viscosity calculated by the magnetohydrodynamic code served as input data to a heat transfer code. The heat transfer code implements the same finite-difference formulation. In the calculations, the Prandtl number was 30 in order to highlight the contribution of the turbulence terms. The results of calculations for the Nusselt number are shown in Fig. 12. The magnetic field increase leads to heat transfer degradation. It also causes longer transition lengths over which the Nusselt number drops to its developed magnitude. The wall-normal field causes more intensive heat transfer reduction because of stronger suppression of turbulence in the free surface region.

## 7. Conclusions and future studies

The model of MHD turbulence and the results presented in the paper reflect a preliminary stage of on-going study. In its present form, the model can be applied to a quite wide class of MHD turbulent flows in closed or open channels. However the model has been adjusted using experi-

mental data, which are restricted to slotted channels or pipes with non-conducting walls and a magnetic field applied perpendicular or parallel to the main flow direction. Hence, it is not apparent to what extent the model is applicable to flows in electrically conducting channels, to those having the aspect ratio of the order of one as well as flows with a multi-component magnetic field. One can expect that the same model without serious modifications can be used in such cases with the dimensionless parameters in the closure expressions built through the effective dimension, such as for example the hydraulic radius. However, further verifications are needed.

Since the mechanism of turbulence suppression by a magnetic field in open and closed channel flows is the same and the characteristic size of vortices generated in these particular flows is controlled by the characteristic channel cross-sectional dimension, the same closure can be used for both open and closed channel flows. However, a test of the applicability of the present model to open channel MHD flows as well as the procedure for the free surface boundary condition will need experimental verifications. To our knowledge, the experimental MHD data suited for testing the model have not been available. The benchmarks will be done in the near future [33].

To the standard limitations of the $K$–$\varepsilon$ model [13] we can probably add one more related to its dissipative properties. In both laminar and turbulent free surface flows, unstable regimes are possible with surface waves propagating downstream or even upstream, which grow in time. Although suppressing instabilities by the applied magnetic field through the induced Lorenz forces is of frequent occurrence, some MHD flows support wave systems in the outer part of the flow even though the magnetic field is strong. Such instabilities in free surface flows with a strong magnetic field were observed experimentally [34] and predicted theoretically [35]. The $K$–$\varepsilon$ model, in general, can be too dissipative to represent accurately such features. Perhaps, the problem is not so pressing in flows where MHD effects are dominant. Such flows have a tendency to form bigger structures. For example, in MHD turbulence "inverse energy cascade" is observed, which results in the turbulence scale increase and gives rise to large energy containing vortical structures aligned in the magnetic field direction. Also, in the presence of a magnetic field long surface waves are mostly responsible for the surface instability [35]. One can expect the representation of such structures is less sensitive to the model dissipation.

The present calculations have shown an importance of the turbulent Prandtl number as a parameter standing for the thermal resistance of a near-surface layer. In the present study, the evaluation of this parameter was based on the experimental data for water flows with Froude number, $Fr$, smaller than one. Such a regime has been known as a "subcritical" flow in which the surface instability does not grow downstream. Rather when subcritical flows, in applications the "supercritical" regime ($Fr > 1$) can occur, which may demonstrate surface renewal and amplification of surface waves. Therefore, further evaluation of this parameter in supercritical flows with and without a magnetic field is needed. These measurements will be performed soon [33].

## Acknowledgements

We gratefully acknowledge the support provided by the US Department of Energy through contract DE-FG03-88ER52150 A008. The authors also wish to express their gratitude to Prof. Hiroshi Kawamura from Science University of Tokyo for useful discussions during the First International Symposium on Turbulence and Shear Flow in Santa Barbara.

## References

[1] M.A. Abdou et al., Exploring novel high power density concepts for attractive fusion systems, Fusion Eng. Des. 45 (1999) 145.
[2] R.W. Moir, Liquid walls for fusion reaction chambers, Comments Plasma Phys. Controlled Fusion, Comments Modern Phys. 2 (2000) 99.
[3] H. Branover, in: Magnetohydrodynamic Flows in Ducts, Wiley, New York, 1978, p. 290.
[4] P.S. Lykoudis, E.C. Brouilette, Magneto-fluid-mechanic channel flow. II. Theory, Phys. Fluids 10 (1967) 1002.
[5] K. Kitamura, M. Hirata, Turbulent heat and momentum transfer for electrically conducting fluid flowing in two-dimensional channel under transverse magnetic field, in: Proceedings of the 6th International Heat Transfer Conference, vol. 3, Toronto, Canada, August 7–11, 1978, pp. 159–164.
[6] Yu. Shimomura, Statistical analysis of magnetohydrodynamic turbulent shear flows at low magnetic Reynolds number, J. Phys. Soc. Jpn. 57 (1988) 2365.
[7] M. Takahashi, A. Inoue, M. Aritomi, M. Matsuzaki, Numerical analysis for laminar and turbulent liquid-metal flow, Fusion Eng. Des. 8 (1989) 249.
[8] A. Inoue, Y. Kozawa, M. Takahashi, M. Matsuzaki, A. Yoshizawa, Characteristics of flow and heat transfer in air-mercury two-phase stratified flow under a vertical magnetic field, Exp. Therm. Fluid Sci. 8 (1994) 46.
[9] S. Cuevas, B.F. Picologlou, J.S. Walker, G. Talmage, Liquid metal MHD flow in rectangular ducts with thin conducting or insulating walls: laminar and turbulent solutions, Int. J. Eng. Sci. 35 (1997) 485.
[10] N. Kasagi et al., DNS database of turbulence and heat transfer. Available from http://www.thtlab.t.u-tokyo.ac.jp/DNS/dns_database.html.
[11] P. Orlandi, Drag reduction in turbulent MHD pipe flows, in: Proceedings of the 1996 Summer Program, Center for Turbulence Research, Stanford, USA, 1996, pp. 447–456.
[12] Yu. Shimomura, Large eddy simulation of magnetohydrodynamic turbulent channel flows under uniform magnetic field, Phys. Fluids l3 (1991) 3098.
[13] D.C. Wilcox, in: Turbulence Modeling for CFD, second ed., DCW Industries, 1998, p. 540.
[14] O. Widlund, S. Zahrai, F.H. Bark, Development of a Reynolds stress closure for modeling of homogeneous MHD turbulence, Phys. Fluids 10 (1998) 1987.
[15] H.-C. Ji, R.A. Gardner, Numerical analysis of turbulent pipe flow in a transverse magnetic field, Int. J. Heat Mass Transfer 40 (1997) 1839.
[16] W. Rodi, Turbulence Models and Their Application in Hydraulics: A State of the Art Review, International Association for Hydraulic Research, Delft, the Netherlands, 1984.
[17] S.B. Pope, in: Turbulent Flows, University Press, Cambridge, 2000, p. 771.
[18] S. Satake, August 2000, private communication.
[19] V.B. Levin, I.A. Chinenkov, Experimental investigations of the turbulent flow of an electrically conducting fluid in a longitudinal magnetic field, Magnetohydrodynamics 4 (1966) 89.
[20] D.S. Kovner, E.Yu. Krasilnikov, Experimental study of turbulent flow of conducing liquid in a pipe under a longitudinal magnetic field, Dokl. Akad. Nauk USSR 163 (1965) 1096 (in Russian).
[21] E.C. Brouillette, P.S. Lykoudis, Magneto-fluid-mechanic channel flow. I. Experiment, Phys. Fluids 10 (1967) 995.
[22] G.G. Branover, A.S. Vasil'ev, Yu.M. Gel'fgat, E.V. Shcherbinin, Turbulent flow in a plane perpendicular to a magnetic field, Magnetohydrodynamics 4 (1966) 78.
[23] V.C. Patel, W. Rodi, G. Scheuerer, Turbulence models for near-wall and low Reynolds number flows: a review, AIAA J. 23 (1985) 1308.
[24] K.-Y. Chien, Predictions of channel and boundary-layer flows with a low-Reynolds number turbulence model, AIAA J. 20 (1982) 33.
[25] W.P. Jones, B.E. Launder, The prediction of laminarization with a two-equation model of turbulence, Int. J. Heat Mass Transfer 15 (1972) 301.
[26] A.K. Rastogi, W. Rodi, Prediction of heat and mass transfer in open channels, J. Hydraul. Div., Proc. Am. Soc. Civil Eng. 104 (HY3) (1978) 397.
[27] L.G. Genin, V.G. Zhilin, Influence of a longitudinal magnetic field on the friction coefficient in a pipe flow of mercury, Teplofi. Vys. Temp. 4 (1966) 233 (in Russian).

[28] F.G. Blottner, Variable grid scheme applied to turbulent boundary layers, Comput. Meth. Appl. Mech. Eng. 2 (1974) 179.
[29] I. Nezu, H. Nakagawa, Turbulence in open-channel flows, IAHR AIRH Monograph Series, 1993, p. 281.
[30] I. Nezu, W. Rodi, Open-channel flow measurements with a laser Doppler anemometer, J. Hydraul. Eng. 5 (1986) 335.
[31] H. Ueda, R. Moller, S. Komori, T. Mizushina, Eddy diffusivity near the free surface of open channel flow, Int. J. Heat Mass Transfer 20 (1977) 1127.
[32] S. Komori, H. Ueda, Turbulence structure and transport mechanism at the free surface in an open channel flow, Int. J. Heat Mass Transfer 25 (1982) 513.
[33] B. Freeze et al., FliHy status (including design and modeling efforts for test article designs), in: APEX Meeting 13, Sandia National Laboratory, November 15–17, 2000.
[34] I. Bucenieks, O. Lielausis, E. Platacis, A. Shishko, Experimental study of liquid metal film and jet flows in a strong magnetic field, Magnetohydrodynamics 2 (1994) 179.
[35] T.N. Aitov, E.M. Kirillina, A.V. Tananaev, Stability of the flow of a thin layer of liquid metal in a coplanar magnetic field, Magnetohydrodynamics 1 (1988) 5.